Deformation-Driven Closed-Chain Soft Mobile Robot Aimed for Rolling and Climbing Locomotion

Luka Paul Johnsen [ID] and Hideyuki Tsukagoshi [ID], *Member, IEEE*

Abstract—The inherent compliance of soft mobile robots makes them a safe option for interaction with humans and fragile environments. To expand their possibilities around our daily life, it is desirable for them to have enhanced traversal ability with safe structure and movement. To meet this requirement, we propose a new type of soft mobile robot that moves while selecting rotational, wave, and climbing locomotion. The proposed robot, named DECSO, forms a closed chain of modular segment actuators that individually generate contraction and bidirectional bending motion by applying negative pressure. In this paper, after presenting methods for generating the above three kinds of locomotion, the characteristics and modeling of the segment actuator are illustrated. Furthermore, the experimental results show that a 4-segment prototype achieved smooth rotational movement in the horizontal plane at a velocity of 75 mm/s, while a 6-segment prototype was able not only to move forward by travelling waves, but also to cross over the human body and obstacles of 62% of its own height by rotational movement. These findings suggest a new possibility for soft mobile robots that can safely touch and move around the human body.

Index Terms—Hydraulic/pneumatic actuators, mobile climbing robots, robot companions, soft actuator modeling, soft robot materials and design.

I. INTRODUCTION

SOCIAL companion robots have shown to be effective in the medical and welfare environments, such as by preventing dementia in the elderly through conversation and health maintenance [1], [2]. However, since the range in which robots themselves can travel while contacting the human body is not sufficient, the area where robots can work is limited [1], [3]. As rigid mobile robots (RMS) have been significantly improved for the last few decades, current versions are relatively agile, and energy saving designs are in progress [4]. However, the lack of flexibility makes it difficult to ensure human safety [5].

Soft mobile robots (SMRs), on the other hand, are easily deformed by their inherent compliance, making them a safe option even in situations involving direct interaction with humans and other vulnerable environments [5], [6]. Numerous designs for terrestrial SMRs were developed, but they are often restricted to one mode of locomotion, and how to enhance the ability of crossing over obstacles has not been discussed enough [5]–[11].

To solve these problems, we propose a new SMR that is inspired by two robot classes: (1) Deformation-driven rolling robots (DDRRs): DDRRs change their shape, resulting in a shift of their center of mass (COM) and center of pressure (COP), which in turn propels the robot forward in a rolling motion. Methods for changing the robot's shape include bending a flexible outer shell [12]–[14], and extending parts of its shell [15]. Although reaching relatively high locomotion speeds, current prototypes cannot climb obstacles because of their restricted deformation capability. (2) Continuum robots: Continuum robots are actuatable structures that move by deformation of a series of constant-curvature arcs [16]. They overcome the limitations of traditional rigid-link structures in terms of adaptability and versatility, allowing them to manipulate objects in complex environments and conform to curvilinear paths in space [16], [17].

Soft linear actuators play a major role in the development of novel SMRs, enabling them to have high degrees of softness [18]. Numerous working principles have been proposed, all having their specific advantages and drawbacks. It proved to be particularly difficult to create linear actuators that combine high deformation, high force, high actuation speed and low mass [18]. Lately, promising artificial muscles driven by negative pressure were created that combine these features [19]–[21], enabling the construction of a new generation of SMRs.

In this study, we introduce a novel SMR that we name Deformation-Driven Closed-Chain Soft Robot (DECSO). It is comprised of modular segment actuators that can actively contract and bend bidirectionally by applying negative pressure, and passively return to their initially elongated state. The segment actuators are smoothly interconnected in a closed chain, which realizes motion through extensive deformation of its body. DECSO has the following three advantages: i) Since it is driven only by negative pressure, there is no concern about explosion or burning. ii) By changing the deformation pattern of the closed chain, the locomotion type can be selected according to the terrain. For example, you can choose options such as circular rotational movement on flat ground, locomotion by traveling waves in narrow gaps, and rotational movement with concave, elongated shapes when traversing obstacles. iii) Since all structures such as actuators for propelling and tubes for energy supply can be constructed with flexible structures, they have good compatibility with the human body.
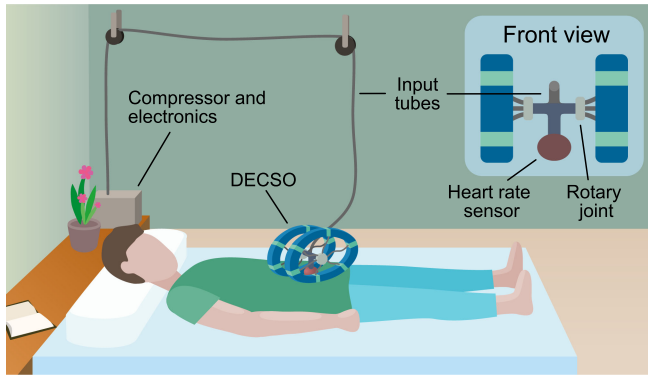
Fig. 1. DECSO application concept. While operating, DECSO could be suspended from the ceiling, move around the body safely, and collect vital signs.

DECSO can be expected to be useful for health management by collecting vital signs while moving around the body of the elderly in bed rest, as shown in Fig. 1. That is, in the non-operating mode, DECSO is supposed to be suspended from the ceiling directly above the bed via a tube. In the operation mode, the tube is lowered to the bed surface, and DECSO can collect signals such as respiration, blood pressure, and pulse while contacting the body.

In this paper, first, we present the methods of circular rotational and traveling wave locomotion on flat ground as well as climbing locomotion by DECSO. Secondly, the characteristics and modelling of DECSOs segment actuators are illustrated. Finally, the locomotion experiments of the developed prototype are shown and the validity of the proposed methods is discussed.

II. METHOD OF FLAT SURFACE AND CLIMBING LOCOMOTION

A. Robot Design

The proposed robot design can be characterized by the following key aspects. Modular and inherently compliant segment actuators (term used interchangeably with "segment") with the same structure and capabilities are connected to form a circular network. The connections do not allow for bending between two segments, but the segments themselves can bend, contract, and elongate by controlling the length of linear actuators on their outer and inner surface (Fig. 2(a)). These small-scale deformations of single segments result in a smooth large-scale deformation of the whole robot (Fig. 2(b)). In general, the segments could be created with any linear actuator that can bend around an axis perpendicular to its axis of active motion. In our case, the segments actively contract and bend by applying negative pressure and passively elongate by returning into their original state.

Under the assumption that the segment's compliance is negligible, the segments can be modeled as circular arcs that have smooth connections, making the robot equivalent to a piecewise circular curve without cusps [22]. Under this consideration, a DECSO consisting of three or less segments is limited to a circular shape that can only change its diameter. Four or more segments on the other hand allow for extensive deformation. In practice however, the segment's compliance does play a major
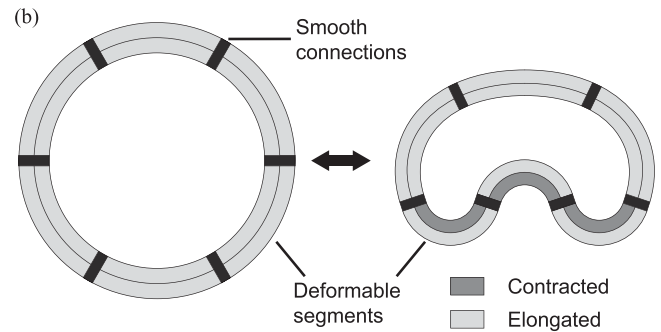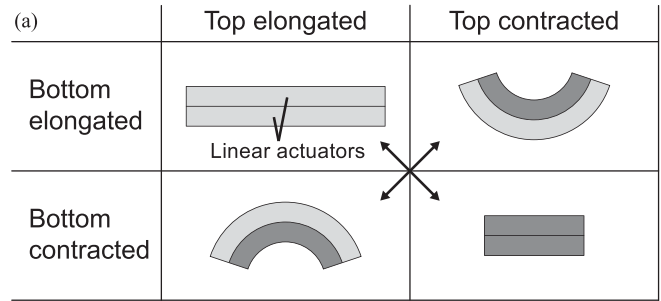

Fig. 2. (a) Each segment deforms by independently contracting (dark gray) and elongating (light gray) its top and bottom actuators, enabling it to elongate, contract, and bend bidirectionally. (b) By combining the segment actuators in a closed chain, deformation of single actuators leads to large-scale deformation of the whole robot.

role in the deformation of DECSO's. High compliance adds to the general safety of the environment by making the robot passively bend around its surroundings, whereas low compliance allows to reliably create shapes. Therefore, the segment's compliance is a trade-off between consistent shape generation and adaptability to its environment.

B. Flat Surface Locomotion

The basic locomotion principle of DECSO's is illustrated in Fig. 3(a). A deformation of the robot to an elliptical shape leads to a change of the center of gravity (COG) and the center of pressure (COP). The distance between the COP and COG creates a torque around the COP that results in a rolling motion around the COP towards a new stable position. Switching between two elliptical shapes leads to a continuous directed rolling locomotion.

Modeling the segment actuators as piecewise circular curve without cusps, four segments are the theoretical minimum to create shapes other than circles and are therefore a minimal requirement for basic rolling locomotion, which is why we chose a four-segment DECSO design to demonstrate this task. It has an input setup as illustrated in Fig. 4 and there are two groups of linear actuators (G1 and G2) that share the same state. The symmetry of the input setup allows to recreate shapes at robot rotations of multiples of one segment (Fig. 4(c)–(d)), making it possible to create two elliptical shapes as is necessary for continuous locomotion. With only one input, it would be possible to create one of the two elliptical shapes in Fig. 3(a). Although this would be enough for one step, the robot could not
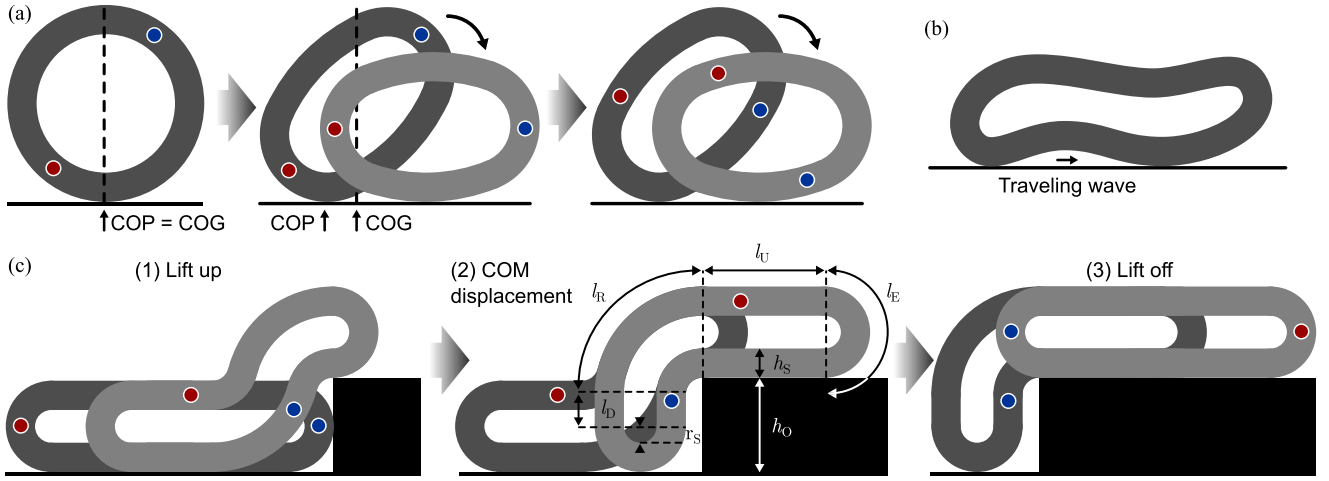
Fig. 3. DECSO locomotion principle. Blue and red dots indicate fixed locations on the robot. Light colored robot shapes follow dark colored ones in regards to time. (a) Basic rolling locomotion principle. (b) Traveling wave locomotion. (c) Climbing locomotion, including (left) Lift up, (center) COM displacement, and (right) lift off phases, as well as (center) the variables for calculating the relationship between DECSO perimeter and obstacle height that can be climbed.
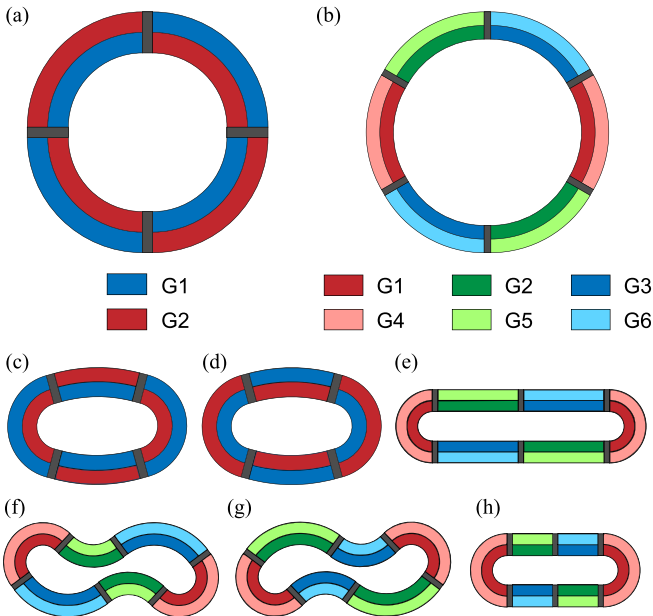

Fig. 4. Input setups for (a) prototype A and (b) prototype B. Same colored linear actuators share the same pressure input, and their respective actuator group names are indicated underneath each prototype's setup. (c, d) Example of input setup symmetry of prototype A. (e-h) Examples of shapes that can be created with prototype B's input setup.

roll any further, making two inputs the minimum requirement for continuous and directed rolling locomotion.

DECSOs are not only able to move forward by infinite rotational motion, but also with traveling waves at the robot's bottom (Fig. 3(b)). Compared to rolling locomotion, crawling has the potential advantages of having a smaller maximal height, and its upper side won't move in opposite direction to its locomotion direction (as is the case during rolling gaits), making it a better option for narrow terrain or when moving underneath objects. The minimum requirement to create a traveling wave on the robot's bottom is to have at least two segments touching the

ground that can bend inwards. Assuming that the segments can bend approximately $180°$ on each side, six segments are the minimum amount of segments needed for traveling wave locomotion.

C. Climbing

The process of climbing onto an obstacle can be divided into three phases as illustrated in Fig. 3(c): (1) Lift up: Part of the robot's body is lifted onto the obstacle. (2) COM displacement: A high portion of the robot is moved onto the obstacle until the robot's COM is above the obstacle. (3) Lift off: The robot lifts off the ground and shifts its entire weight onto the obstacle. This is the most critical part of the climbing process, and if the COM is not above the obstacle the robot will lose contact and fall back onto the ground. We developed a simple theoretical approach to approximate the relationship between the perimeter of DECSO's and the height of a step obstacle it could climb. Assuming that DECSOs can bend at any location of its perimeter with a bending radius specific to the segment actuator, one simple condition to ensure that the COM is on top of the obstacle is when half of the DECSO's body is above the obstacle. The maximal perimeter l_P of the DECSO is

$$l_P = 2(l_U + l_D + l_R + l_E). \tag{1}$$

For the corresponding variables please refer to Fig. 3(c). Note that l_R is considered twice as the section on the other side is in a contracted state and would have the same length in an elongated state. The aforementioned condition holds if

$$2l_U + l_E \geq \frac{1}{2}l_P. \tag{2}$$

Solving this geometrical problem for l_P, the obstacle height h_O, the segment height h_S, and the segment radius r_S, leads to the following height a given DECSO could climb.

$$h_O \leq \frac{l_P}{4} - \left(\frac{5\pi}{4} - 1\right)h_S - \left(\frac{7\pi}{4} - 2\right)r_S \tag{3}$$

To climb obstacles, it is important for DECSOs to have concave shape sections so they can stay in contact with the obstacle and more effectively shift their COM. Although in theory it is possible to create concave robot shapes with only four segments, it would require impractically high differences between segment lengths [22]. Using five segments reduces the requirements on the segment actuators, but the odd number of segments prevents the creation of symmetric input setups that require only a small number of input lines. We decided to use a six-segment DECSO design to approach this task because its higher symmetry allows for simpler input setups. The input setup is illustrated in Fig. 4(b). For segments that are on opposing sides, the inside and outside linear actuators always share the same state, requiring up to six input lines. The input setup allows for creation of many shapes, including concave sections that are necessary for climbing (Fig. 4(e)–(h)). By using only the inside actuator groups (G1-G3), elliptical shapes can be generated that leave the robot's center segments in an elongated, compliant state (Fig. 4(e), Section III), allowing for passive adaptation to small obstacles. Similar to the four-segment input setup, the symmetry of the input setup allows to recreate all shapes at robot rotations of multiples of one segment.

III. SEGMENT ACTUATOR

We decided to use fluid-driven origami-inspired artificial muscles (FOAMs) [20] as linear actuators because they combine high deformation, high force, high actuation speed, low mass, passive elongation, and variable compliance depending on their state. FOAMs are a particularly safe option because of the sole use of negative pressure which has no risk of explosion. The segment actuators used in this study are comprised of two interconnected FOAMs that contract when negative pressure is applied, and elongate passively into their original length. Because the linear actuators are controlled independently, the segment actuator can deform in a combination of both contraction and bending on a large scale (Fig. 5(a)). Each FOAM is comprised of a skeleton that has a structure of angled plates, and a flexible airtight film that surrounds the skeleton. When negative pressure is applied to the linear actuator, the film bends towards the chamber, the angle between the plates decreases, and the actuator volume reduces. The mechanical connection between change in actuator volume and actuator length results in a contraction force. When the actuator contracts, the skeleton and the surrounding film become compressed, resulting in elongation forces that return the actuator to its initial condition.

When in a contracted state, FOAMs are relatively incompliant as extension results in strong contraction forces due to the pressure difference, and further compression results in strong elongation forces as the skeleton is already folded to its maximum. When in an elongated state on the other hand, FOAMs are relatively compliant due to the absence of pressure difference, whereas stretching and contraction of the skeleton in its initial condition results in only small forces.
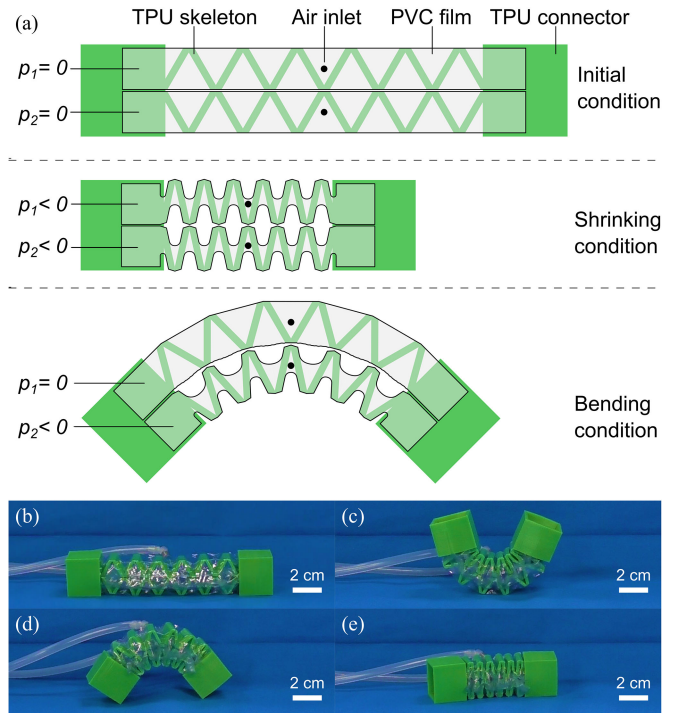

Fig. 5. (a) Each segment actuator consists of two FOAMs that contract when negative pressure is applied. Compared to the initial condition (top), negative pressure in both actuators results in a shrinking condition (middle), whereas negative pressure in only one actuator results in a bending condition (bottom). (b - e) The segment actuator's deformation capabilities with either -60 kPa (contracted) or atmosphere (elongated) as input for each linear actuator. (b) Both elongated. (c) Top contracted, bottom elongated. (d) Top elongated, bottom contracted. (e) Both contracted.

A. Modeling

Analytical modeling of the actuators used in a robot help in the robot's characterization and design process. Although a simplified mechanical model for FOAMs already exists, it is only valid for a preloaded actuator, a correction term was used to fit the model to the experimental data, and the film was assumed to remain at constant length, bend inwards in an unrealistic shape, and have no resistance to compression [20]. To generalize the actuator's behavior over a wider range of design parameters and to help the segment actuator design process, we created a more sophisticated model. The actuator design parameters are shown in Table I. For some equations, intermediate steps are left out or not all variables are broken down to the design parameters. In these cases, please contact the authors for a more detailed explanation.

A single FOAM's blocked force F has three components.

$$F = F_C + F_S + F_F \qquad (4)$$

Here, F_C, F_S and F_F represent a contraction force due to pressure differences inside and outside of the actuator, elongation force due to skeleton compression, and elongation force due to film folding at high contractions, respectively. The actuator can be considered as N equal sections connected in series, and the forces can be modeled using only one section as illustrated in Fig. 6(a). F_C can be calculated using the principal of virtual

TABLE I
ACTUATOR DESIGN PARAMETERS

| Symbol	Design parameter	Value used
W	Skeleton width	18 mm
D	Skeleton plate length	13 mm
θ_0	Initial skeleton angle	30 °
T_S	Skeleton thickness	2 mm
T_H	Skeleton hinge thickness	0.8 mm
E_S	Skeleton tensile modulus	12 MPa
N	Number of skeleton folds	12
T_F	Film thickness	0.1 mm
E_F	Film tensile modulus	1500 MPa
k_L	Film length factor	1.18
δ_F	Film folding start	3.5 mm
k_F	Film folding factor	7×10^5
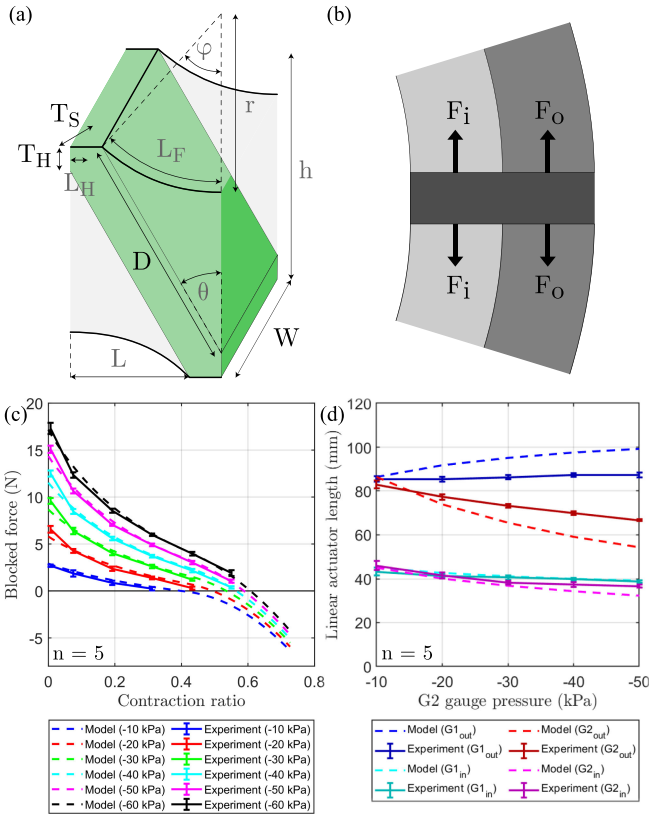
Fig. 6. (a) Isometric view of FOAM section used for modeling. Actuator design parameters and modeling variables are illustrated in black and gray, respectively. (b) At the connections between segments (Fig. 4(a)), each linear actuator exerts a force towards its longitudinal axis that acts in its center. (c) Comparison of isobaric blocked force between model calculation and mean experimental values from five trials, with error bars denoting one standard deviation. (d) Comparison of linear actuator length between model calculation and mean of experiments from five trials, with error bars denoting one standard deviation. During the experiment, constant pressure was applied to G1 (-10 kPa) while the pressure in G2 was varied.

work, where a change in volume inside the actuator dV corresponds to a linear movement dL.

$$F_C(\varphi) = -p \frac{dV(\varphi)}{dL(\varphi)} = -p \frac{dV(\varphi)/d\varphi}{dL(\varphi)/d\varphi} \tag{5}$$

Here, p denotes the pressure difference between the actuator's inside and outside. Unlike in [20], the film is modeled to stretch due to p and bend inwards in a circular shape with an angle φ (the model's dependent variable).

$$L_F = D k_L \sin(\theta_0) \left(1 - \frac{rp}{T_F E_F}\right) \tag{6}$$

Here, each parameter is defined as follows: D: Skeleton plate length, k_L: Film length factor, θ_0: Initial skeleton angle, T_F: Film thickness, E_F: Film tensile modulus. Depending on whether the film touches the skeleton's inside or not (denoted by subscripts "1" and "2," respectively), F_C is calculated differently.

$$F_{C1} = -pW \left(\sqrt{D^2 - L^2} \left(1 - \frac{L^2}{D^2 - L^2}\right) \right.$$
$$\left. -r \frac{1 - \cos(2\varphi) - \frac{r}{Dk_L \sin(\theta_0)}(2\varphi - \sin(2\varphi))}{\cos(\varphi) - \frac{r\sin(\varphi)}{Dk_L \sin(\theta_0)}} \right) \tag{7}$$

$$F_{C2} = -\frac{pWr^2 \sin(\varphi)}{D \cos^2(\varphi)} \left(\frac{2r \left(\frac{\sin^3(\varphi)}{\cos(\varphi)} + \frac{\sin(2\varphi)}{2} - \varphi \right)}{D - Dk_L \sin(\theta_0)} - 1 \right) \tag{8}$$

Here, W and L represent the skeleton width and the segment length, respectively. Whereas [20] used a simple cantilever-spring model for F_S, we use Castigliano's first and second theorems to integrate over the different sections of the skeleton plates.

$$F_S = -\frac{(D \sin(\theta_0) - L)E_S W}{2D^2 \cos^2(\theta_0) \left(\frac{3L_H(T_S + T_H)}{2 T_S^2 T_H^2} + \frac{D}{T_S^3} \right)} \tag{9}$$

Here, each parameter is defined as follows: E_S: Skeleton tensile modulus, L_H: Skeleton hinge length, T_S: Skeleton thickness, T_H: Skeleton hinge thickness. For calculation of F_F, a quadratic relationship between F_F and the section contraction δ is used. It starts at the section contraction δ_F and its strength is determined by the film folding factor k_F.

$$F_F = -k_F (\delta - \delta_F)^2 \tag{10}$$

The actuator's contraction ratio C_R can be determined with the current and initial linear actuator lengths L_A and L_{A0}, respectively.

$$C_R = \frac{L_{A0} - L_A}{L_{A0}} \tag{11}$$

$$L_A = N \left(D \sin(\theta) + \frac{T_S}{\cos(\theta)} - T_H \tan(\theta) \right) \tag{12}$$

Here, N and θ denote the number of skeleton folds and the skeleton hinge angle, respectively. (12) becomes L_{A0} when $\theta = \theta_0$. The segment's bending angle β depends on the segment's outside and inside linear actuator lengths L_{Ao}, L_{Ai} and heights h_o, h_i, respectively.

$$\beta = \frac{L_{Ao} - L_{Ai}}{h_o + h_i} \tag{13}$$

We further introduce a heuristic that approximates the overall DECSO shape from the linear actuator's pressures. The linear actuators are assumed to have no resistance to bending, and their force to act in the middle of the actuator and to be equal to the actuators force during an unbent shape at the length on the segment's outside and inside, respectively (Fig. 6(b)). As the force at both ends of each linear actuator has the same absolute value, these assumptions result in the following condition for robot shape equilibrium.

$$F_o = -F_i \qquad (14)$$

Here, F_o and F_i represent the force of all outside actuators and the force of all inside actuators, respectively. If there exists an explicit value for the actuator length for a given F, the linear actuator lengths can be found by iterating through all possible values for F_o and searching for the condition when the total bending angle of all segments equals 2π.

In order to achieve high DECSO deformation and shape controllability, the following requirements for the segment actuators have been identified. (R1): High bidirectional bending capability, (R2): High contraction ratio, (R3): High contraction forces, (R4): High elongation forces, (R5): Small weight, and (R6): High deformation speed. To reach high values for (R1), (13) shows that a decrease in height and an increase in actuator contraction ($L_{Ao} - L_{Ai}$) will improve the bending capability. (12) shows that the actuator contraction can be adjusted with N without affecting actuator forces and contraction ratio, as N is not part of (7)–(10) and cancels out in (11). (R2) can be increased by maximizing D and θ_0 and minimizing T_S and T_H as indicated by (11) and (12) with $L_A(\theta = 0)$. For enhancing (R3), considering (7) and (8), high values for W are clearly beneficial, whereas high values for D, T_F and E_F as well as low values for θ_0 are suspected to be beneficial but require more consideration, e.g. by using an optimization algorithm. High (R4) can be achieved by increasing E_S and W and decreasing in D as pointed out in (9). Whereas not clearly shown by (9), we suspect that higher T_H and T_S also result in an increase of F_S. (R5) can be decreased by reducing the overall actuator size and density of materials used, and (R6) can be increased by reducing the actuator's initial volume by minimizing N, W, and D and choosing θ_0 to be either high or low (maximal volume at $\theta_0 = 45°$).

The actuator force model and the shape approximation model were validated empirically, and all experiments were repeated five times. The FOAM's blocked force in relation to its contraction ratio was compared to the calculation of the introduced model. The actuator length was fixed to decreasing values, and at each length, the blocked force was measured at 10 kPa intervals between -10 kPa and -60 kPa. The FOAM model calculations are in good agreement with the experimental data over the whole contraction, showing an average model error of approximately 0.37 N or 2.1% of the highest experimental mean value (17.3 N) (Fig. 6(c)). To validate the robot shape approximation, with PA (section IV-A) in horizontal position, the pressure of G2 (Fig. 4(a)) was slowly decreased in 10 kPa intervals between -10 kPa and -50 while keeping G1 at -10 kPa. Each segment's outside and inside lengths were determined using manual tracking

with ImageJ (v.1.52p) and compared to the shape approximation model. When G1 and G2 are both at -10 kPa, the robot's shape is described well by the model. Both model and experiments show similar qualitative behavior, with the values for model and experiment drifting apart with decreasing G2. The average model error is approximately 4.77 mm or 7.9% of the overall mean of all empirical measurements (Fig. 6(d)).

B. Construction

The actuator parameters used for actuator creation can be seen in Table I. E_S, E_F, and T_F were determined by the materials used and were chosen during early development. W, D, θ_0, T_S, T_H, and N were designed according to the knowledge gained through the modeling, and multiple actuators were created until the segment's performance was satisfying and the deformation capability came close to the robot shapes from Fig. 4(c)–(h). k_L was estimated by the authors after actuator creation, and δ_F and k_F were manually fitted to the experimental results during model validation.

The actuator skeletons were 3D printed using a Replicator 2X 3D printer with NinjaFlex thermoplastic polyurethane (TPU) filament. Polyvinyl chloride films were placed underneath and above the skeleton and heat sealed with an impulse sealer at the actuator's sides to create an airtight skin, leaving space for a TPU tube that was glued into the opening. For segment creation, two linear actuators were combined by heat sealing their sides (which stuck out from linear actuator creation) together and plugging them into 3D printed TPU frames. There is no physical bond between the linear actuator's films at their intersection (Fig. 5(a)). Each segment actuator was 104 mm long, 27 mm high, and had a mass of 33 g. When a gauge pressure of -60 kPa was applied to the respective linear actuators with a negative pressure pump (flowrate: 4 l/min), the segment actuators produced a contraction ratio of their active part of about 0.58 and a bending angle of about 145° to either side with a bending radius of 13 mm (Fig. 5(b)-(e)).

IV. LOCOMOTION EXPERIMENTS

A. Setup

Two DECSO prototypes were created by connecting the segments in a circular shape with TPU frames. Prototype A (PA) consisted of four segments with a mass of 230 g and a diameter of 123 mm - 163 mm (perimeter: 387 mm - 512 mm) when all segments were contracted or elongated, respectively. Prototype B (PB) consisted of six segments, had a mass of 350 g, and a diameter of 154 mm - 242 mm (perimeter: 484 mm - 760 mm). Both DECSO prototypes were controlled solely with negative pressure inputs of either -60 kPa or atmosphere according to the input setup in Fig. 4(a) and (b). The prototype's main component, the skeleton, has a tensile modulus of 12 MPa, which lies approximately in the center of the spectrum of currently existing soft robots [6], and the actuator's zigzag architecture as well as the ring-like configuration of DECSOs further promote the system's structural compliance. As such, the prototype's softness can be

Fig. 7. Sequential Images of results for locomotion experiments. (a-l) Each image stands for one state input, and start and finish time are shown in the first and last images, respectively. Pressure input is indicated with dark gray = -60 kPa and light gray = atmosphere. (a-c) Rolling locomotion with four segments and two inputs. (d-f) Traveling wave locomotion with six segments and six inputs. (g-l) Step climbing with six inputs. (m-n) Passive compliance while overcoming small obstacles with three inputs. (o-t) Climbing the human body while keeping a soft touch.

categorized as tier 3: Entirely soft robots relying on external hard components [6].

The DECSO locomotion principles as introduced in Fig. 3 were tested experimentally. The obstacles for climbing included a rounded obstacle of 25 mm height, a step of 50 mm height, as well as a human arm (height: 50 mm), and torso in bed rest (height: 190 mm). Please note that the test subject sunk into the mattress which reduced the effective height of the torso. The speed, climbing ability, and adaptability through changing modes of locomotion was then compared to other DDRRs and well known robots with comparable degree of softness [9], [11]–[14].

B. Results and Discussion

The sequential images of the locomotion experiments are shown in Fig. 7. For some locomotion tasks, the locomotion

patterns (sequence of linear actuator input states) are illustrated within the respective image. For a detailed view of the locomotion patterns please refer to the supplementary video.

On flat ground, PA performed directed continuous locomotion by switching between one circular and two elliptical states. Switching to a circular shape in between the elliptical shapes let the robot use its momentum gained and keep rolling before the next elliptical state was applied. Starting from a resting position, the average speed and speed-diameter ratio during two steps were approximately 75 mm/s and 0.67 s^{-1}, respectively. After more than two steps however, PA fell to a side because the connecting tubes started pulling on PA due to the tubes twisting and the vacuum pump being stationary. PB could move with a basic rolling gait while varying its length (supplementary video), and also with a traveling wave locomotion by periodically switching between one elliptical and two concave shapes. The traveling wave propagated from the bottom back segment to the bottom front segment, propelling the robot forward at a velocity of approximately 3.5 mm/s. PB's characteristic height and length of 81 mm and 241 mm were measured from its shape in Fig. 7(d).

PB was able to climb over the rounded obstacle with a three input rolling gait that contracts only the inside linear actuators. The elongated bottom segments that were in contact with the obstacle bent outwards due to their high compliance, passively adapting to the obstacle's shape and creating a high contact area. With the same gait, PB could overcome the human arm of 61% of its own height in 16.4 s while keeping a high contact area. Using all six inputs enabled PB to climb the step obstacle of 50 mm height (62% of its own height). Switching between the concave shapes (Fig. 4(f), (g)) was effective for the COM displacement phase, whereas shrinking the robot's length was effective for the critical lift off phase. The segments in an elongated state showed high compliance, which led to major differences in robot shape when comparing two equal states during different phases of the climbing process (Fig. 7(h), (j)). Inserting the values of $l_P = 512$ mm, $h_S = 27$ mm, and $r_S = 13$ mm into (3) results in a theoretical maximum obstacle height of 65.5 mm for the dimensions of PB. Compared with the 50 mm step actually climbed, PB was able to climb an obstacle of 76% of the height a DECSO with no restriction of bending locations (due to number of segments and input lines) could climb in theory. With similar climbing patterns, PB was also able to overcome a human torso in lying position (Fig. 7(r)–(t)). For the initial climbing onto the torso, the same climbing pattern as for the step obstacle was effective. After that, alternating between the two concave robot states (Fig. 4(f), (g)) let PB overcome the center part of the torso. For going down, the basic rolling gait that was used for the rounded obstacle was effective. The results of this study show that the robot's dimensions, the number of segments and input lines, as well as the linear actuator's construction parameters are generally in a good range for the application as a companion robot that is able to traverse people in bed rest.

Our prototype's speed and climbing capability in comparison to other soft and deformation driven robots is shown in Table II, where PA was used for speed related values and PB for all others of this work. The softness scale from [6] reaches from 1 to 4,

TABLE II
PERFORMANCE COMPARISON OF SOFT AND DEFORMATION-DRIVEN ROBOTS

Characteristic	This work	Tolley et al. [9]	Usevitch et al. [11]	Sugiyama & Hirai [12]	Masuda & Ishikawa [13]	Li et al [14]
Climbing: Obstacle to robot height ratio	0.62	-	-	-	-	-
Degree of softness (quantified with [6])	3	2	2	2	2	3
Multiple locomotion principles	Yes	Yes	No	Yes	No	No
Robot speed to length ratio in s^{-1}	0.67	0.007	0.036	0.65	2.65	0.73
Robot speed to mass ratio in $mm\,s^{-1}\,g^{-1}$	0.3	0.001	0.002	8.6	2.3	41.22

with 1 denoting a hard robot modified to perform compliant behavior and 4 being a completely soft untethered robot. The values for other works were partially calculated from other values when the compared values were not stated in the research. In comparison, the prototypes created here have medium speed in relation to their size and mass, while outperforming all other compared robots in climbing ability, and having similar or better performance in degree of softness as well as adaptability through multiple modes of locomotion. Although SMRs with higher speed already exist, the authors were not able to find any robot with comparable softness and scale that was reported to climb obstacles. We suspect the higher overall deformation capability to be the main reason for the superior climbing performance and adaptability compared to prior DDRRs, and especially the ability of DECSOs to create concave shapes appears to be a key for effective climbing.

V. CONCLUSION AND FUTURE WORK

A new concept for a soft mobile robot with rolling locomotion called DECSO was proposed, aimed for high compatibility with the lying human body. To realize it, a driving method using segment actuators with high contraction by negative pressure was introduced, and its characteristics were investigated by a mathematical model. The validity of the proposed methods were verified experimentally by DECSO prototypes. We plan to extend the proposed method to a structure of two wheels, which is expected to steer the direction even on the human body by using the advantage of its light structure and softness. A rotary union could be used to prevent the tether from twisting, allowing the robot to freely change its location. We would also plan to consider the possibility of acquiring vital signals by mounting a sensor that detects pulse and breath sounds in the part that exists between the two chains.

REFERENCES

[1] I. Pedersen, S. Reid, and K. Aspevig, "Developing social robots for aging populations: A literature review of recent academic sources," *Sociol. Compass*, vol. 12, no. 6, 2018, Art. no. e12585.

[2] N. Geva, F. Uzefovsky, and S. Levy-Tzedek, "Touching the social robot paro reduces pain perception and salivary oxytocin levels," *Sci. Rep.*, vol. 10, no. 1, pp. 1–15, 2020.

[3] J. Broekens et al., "Assistive social robots in elderly care: A review," *Gerontechnol.*, vol. 8, no. 2, pp. 94–103, 2009.

[4] F. Rubio, F. Valero, and C. Llopis-Albert, "A review of mobile robots: Concepts, methods, theoretical framework, and applications," *Int. J. Adv. Robotic Syst.*, vol. 16, no. 2, 2019, Art. no. 1729881419839596.

[5] D. Rus and M. T. Tolley, "Design, fabrication and control of soft robots," *Nature*, vol. 521, no. 7553, pp. 467–475, 2015.

[6] K. Chubb, D. Berry, and T. Burke, "Towards an ontology for soft robots: What is soft," *Bioinspiration Biomimetics*, vol. 14, no. 6, 2019, Art. no. 063001.

[7] M. Calisti, M. Cianchetti, M. Manti, F. Corucci, and C. Laschi, "Contest-driven soft-robotics boost: The robosoft grand challenge," *Front. Robot. AI*, vol. 3, 2016, Art. no. 55.

[8] H.-T. Lin, G. G. Leisk, and B. Trimmer, "GoQBot: A caterpillar-inspired soft-bodied rolling robot," *Bioinspiration Biomimetics*, vol. 6, no. 2, 2011, Art. no. 026007.

[9] M. T. Tolley et al., "A resilient, untethered soft robot," *Soft Robot.*, vol. 1, no. 3, pp. 213–223, 2014.

[10] M. A. Robertson and J. Paik, "New soft robots really suck: Vacuum-powered systems empower diverse capabilities," *Sci. Robot.*, vol. 2, no. 9, 2017, Art. no. eaan6357.

[11] N. S. Usevitch, Z. M. Hammond, M. Schwager, A. M. Okamura, E. W. Hawkes, and S. Follmer, "An untethered isoperimetric soft robot," *Sci. Robot.*, vol. 5, no. 40, 2020, Art. no. eaaz0492.

[12] Y. Sugiyama and S. Hirai, "Crawling and jumping by a deformable robot," *Int. J. Robot. Res.*, vol. 25, no. 5/6, pp. 603–620, 2006.

[13] Y. Masuda and M. Ishikawa, "Development of a deformation-driven rolling robot with a soft outer shell," in *Proc. IEEE Int. Conf. Adv. Intell. Mechatronics*, 2017, pp. 1651–1656.

[14] W.-B. Li, W.-M. Zhang, H.-X. Zou, Z.-K. Peng, and G. Meng, "A fast rolling soft robot driven by dielectric elastomer," *IEEE/ASME Trans. Mechatronics*, vol. 23, no. 4, pp. 1630–1640, Aug. 2018.

[15] E. Steltz, A. Mozeika, N. Rodenberg, E. Brown, and H. M. Jaeger, "JSEL: Jamming skin enabled locomotion," in *Proc. IEEE/RSJ Int. Conf. Intell. Robots Syst.*, 2009, pp. 5672–5677.

[16] J. Burgner-Kahrs, D. C. Rucker, and H. Choset, "Continuum robots for medical applications: A survey," *IEEE Trans. Robot.*, vol. 31, no. 6, pp. 1261–1280, Dec. 2015.

[17] I. D. Walker, "Continuous backbone 'continuum' robot manipulators," *Int. Scholarly Res. Notices*, vol. 2013, 2013, Art. no. 726506.

[18] J. Zhang et al., "Robotic artificial muscles: Current progress and future perspectives," *IEEE Trans. Robot.*, vol. 35, no. 3, pp. 761–781, Jun. 2019.

[19] J.-G. Lee and H. Rodrigue, "Origami-based vacuum pneumatic artificial muscles with large contraction ratios," *Soft Robot.*, vol. 6, no. 1, pp. 109–117, 2019.

[20] S. Li, D. M. Vogt, D. Rus, and R. J. Wood, "Fluid-driven origami-inspired artificial muscles," *Proc. Nat. Acad. Sci. USA*, vol. 114, no. 50, pp. 13132–13137, 2017.

[21] J.-G. Lee and H. Rodrigue, "Armor-based stable force pneumatic artificial muscles for steady actuation properties," *Soft Robot.*, vol. 9, pp. 413–424, 2022.

[22] T. Banchoff and P. Giblin, "On the geometry of piecewise circular curves," *Amer. Math. Monthly*, vol. 101, no. 5, pp. 403–416, 1994.